J Geophys (1983) 54:35–50

Journal of Geophysics

Geomagnetic induction studies in Scandinavia

III. Magnetotelluric observations

A.G. Jones[1,2],* B. Olafsdottir[2] and J. Tiikkainen[3]

[1] Institut für Geophysik, Corrensstraße 24, D-4400 Münster, Federal Republic of Germany
[2] Swedish Geological Survey (SGU), Box 670, S-751 28 Uppsala, Sweden
[3] Department of Geophysics, Oulu University, SF-90570 Oulu, Finland

Abstract. In this work, data from two of the instruments of the Münster International Magnetospheric Study (IMS) Scandinavian Magnetometer Array are combined with synoptic telluric field measurements, and the joint data sets are analysed to derive the magnetotelluric response functions for the locations. The data analysis procedures employed, particularly the timing error correction technique, are described in detail. One-dimensional interpretations of the response functions, from both the northern Swedish and the southern Finnish location, are shown to be valid. Accordingly, both first-approximation continuous models and more comprehensive layered-earth models – found by a Monte-Carlo search procedure – acceptable to the response functions are illustrated. The models acceptable to the northern Swedish MT response are almost identical to those acceptable to the previously derived horizontal spatial gradient (HSG) response for the same locale, displaying a monotonically decreasing electrical resistivity with depth, and the existence of a zone of low resistivity in the upper mantle at a depth of around 200 km. For the southern Finnish data however, the acceptable models describe the existence of a lower crustal conducting layer, of around 25 Ωm, which was suspected from a qualitative analysis of previous work. Inadequate and insufficient long period information for this location preclude a positive identification of a possible electrical asthenosphere beneath southern Finland. However, any such zone cannot be closer to the surface than 150 km.

Key words: Geomagnetic induction studies in Scandinavia – Magnetotelluric data analysis – International Magnetospheric Study – Electrical asthenosphere – ELAS project

1. Introduction

Geomagnetic induction effects observed by the Scandinavian IMS (International Magnetospheric Study) magnetometer array (Küppers et al., 1979) have been discussed in two previous publications in this series (Jones, 1980 and Jones, 1981a, hereafter referred to as Papers I and II respectively), and in two associated works (Jones, 1982a and Jones, 1982b, Papers Ia and Ib). The analyses of the magnetometer data alone, by both the horizontal spatial gradient (HSG) method and the more traditional geomagnetic depth sounding (GDS) methods, were quite successful in detailing the upper mantle (i.e., depths <200 km) 1*D* conductivity structure beneath northern Sweden (Papers I, Ia, Ib) and northern Finland/northeastern Norway (Paper Ib), and in delineating two rather strong inhomogeneities in electrical conductivity, probably in the crust, in northern Norway and northern Sweden (Paper II). The latter of these, the Storavan anomaly, was also observed by Richmond and Baumjohann (1983) in their internal/external separation of the magnetometer array data.

In this work, magnetic observations recorded by two instruments of the array are combined with telluric measurements made at the same locations, and the joint data sets are analysed in order to derive the magnetotelluric (MT) response functions for those locations. At one of the locations, audiomagnetotelluric measurements were also made. Attention is given to the analysis methods employed, and a general technique for reducing any possible timing discrepancy between the telluric and magnetic data sets is described and utilized. Models consistent with the resulting MT response functions from the two locations are discovered by a Monte-Carlo random search of the parameter spaces, and resistivity-depth profiles are presented. The acceptable models are shown to be highly compatible to those for the HSG data.

Other geomagnetic induction experiments have recently been conducted in Finland. Ádám et al. (1982a) made MT measurements at five locations along a SW/NE profile, with an average inter-station spacing of some 60 km. Ádám et al. (1983), complementing the above work with two long period (10^3–10^4 s) MT sites, compared the results of their experiment with similar ones conducted in the Pannonian basin. Pajunpää et al. (in press 1983) have presented a prelimenary interpretation of one of their magnetometer array studies which straddled the Ladoga-Bothnian Bay zone (see Fig. 1). These works will be compared with the present results in Sect. 7.

* *Present address:* Geophysics Laboratory, Physics Department, University of Toronto, Toronto, Ontario, Canada, M5S 1A7

Offprint requests to: Dr. A.G. Jones

The four MT components will be referred to by the following letters or subscript numbers:

component	*letter*	*subscript*
magnetic north	*h* or *H*	1
magnetic east	*d* or *D*	2
telluric north	*n* or *N*	3
telluric east	*e* or *E*	4

(this numbering convention was introduced by Reddy and Rankin, 1974) where "north" and "east" refer to the Kiruna cartesian co-ordinate system introduced in Küppers et al. (1979); small letters refer to time domain series and parameters, whilst capital letters refer to frequency domain series and parameters throughout.

2. Instrumentation

2.1 Magnetic instrumentation

The three components of the time-varying magnetic field were recorded on photographic film by modified Gough-Reitzel magnetometers (Gough and Reitzel, 1967; Küppers and Post, 1981) located in Scandinavia principally for observations during the IMS, to which Münster University contributed by operating an array of 36 instruments. Full details of the array can be found in Küppers et al. (1979), and of the instruments in Küppers and Post (1981). The magnetic resolution of the variometers was assessed at approximately 2nT for a digitization accuracy of one millimeter, and the temporal resolution was typically better than 20s for an instrument on 10s recording mode (the problems encountered due to timing discrepancies between the telluric and magnetic data are discussed in detail in Sect. 4.4).

The response functions of the three wire-suspended magnets for a typical magnetometer are illustrated in Küppers and Post (1981). The copper (Cu) damping blocks around each magnet acted quite closely as first-order low pass Butterworth filters (see, for example, Kulhánek, 1976, pp. 87–92) with −3 dB points for a typical instrument at periods of:

h-component: 9.5 s,
d-component: 13.0 s,
z-component: 5.5 s.

Hence, correction for instrument response was undertaken in the frequency domain by multiplying each complex Fourier harmonic of the magnetic data with the term

$$1+i\frac{\omega}{\omega_c} \tag{1}$$

where ω_c is the appropriate −3 dB point frequency given above. (Note that because the −3 dB point frequencies are all above the Nyquist frequency, equal to a period of 20 s for an instrument on 10 s mode recording, this correction cannot be applied in the time domain due to aliasing effects. For correction of the time domain series, which may be necessary for investigations of short period phenomena, e.g., pulsation studies (Glaßmeier, 1980), the series must be Fourier transformed, the relevant correction (as given by Eq. 1) applied, then the corrected series must be inverse Fourier transformed. This latter set of operations is also significantly faster than correction in the time domain by convolution filtering (see, for example, Rader, 1970).)

2.2 Telluric instrumentation

The telluric observations were made by a single two-component instrument. The equipment was of simple design and construction, and, apart from the timing clock, the two channels were independent of each other. For each channel, the signals, recorded by the pairs of electrodes (constructed of lead (Pb) at NAT, and copper sulphate ($CuSO_4$) at SAU, see Fig. 1), were electronically processed by the following set of operations:

(a) common mode rejection,

(b) band-pass filtering, by coupled low-pass and high-pass single pole passive RC circuits, with a resonance period of 922.6 s and an amplitude drop-off of 6 dB/octave,

(c) amplification, by Keithley low noise amplifiers, and

(d) analogue recording, by Minigor paper chart writers.

The system also included an internal quartz clock, and was battery powered such that an uninterrupted recording of 48 h of data was possible. This latter time was, however, dependent on the chart speed chosen. The usual chart speed was 15 cm/h, i.e., 12 s/mm, but occasionally a faster speed of 30 cm/h was used, in which case continuous recording of approximately 36 h of data was obtained. The clock was always started with reference to a transmitted radio timing signal (as were the magnetometers).

As described in *(b)*, the data were band-pass filtered. Correction for this was undertaken in the frequency domain (for the computational reasons detailed above) by multiplying each Fourier harmonic of the telluric data with the term:

$$10.244+i\left(8599\omega-\frac{1}{3908\omega}\right) \tag{2}$$

where ω is the frequency of interest (in units of s^{-1}).

2.3 AMT instrumentation

Audiomagnetotelluric (AMT) observations were made in addition in the vicinity of Sauvamäki (see Fig. 1) with a French scalar system ECA 541-0, manufactured by Société Eca of Paris. The equipment was originally developed at the Centre de Récherches Géophysiques, Garchy (Benderitter et al., 1973). The amplitudes of the telluric and magnetic fields were measured, at nine fixed frequencies, from 8–3,700 Hz. Two induction coils were used, one for the lower band (8–370 Hz), and one for the upper band (170–3,700 Hz), of frequencies. The telluric field was measured galvanically using steel electrodes. After integration and electronic division of the amplitudes, the scalar value of apparent resistivity at each frequency was read directly from the instrument. At least five such readings were usually taken at each frequency and for each orientation. For every reading, the two signal amplitude meters (one for each of the magnetic and telluric fields) were monitored during the integration period to ensure that a reasonable correlation was present between the fields.

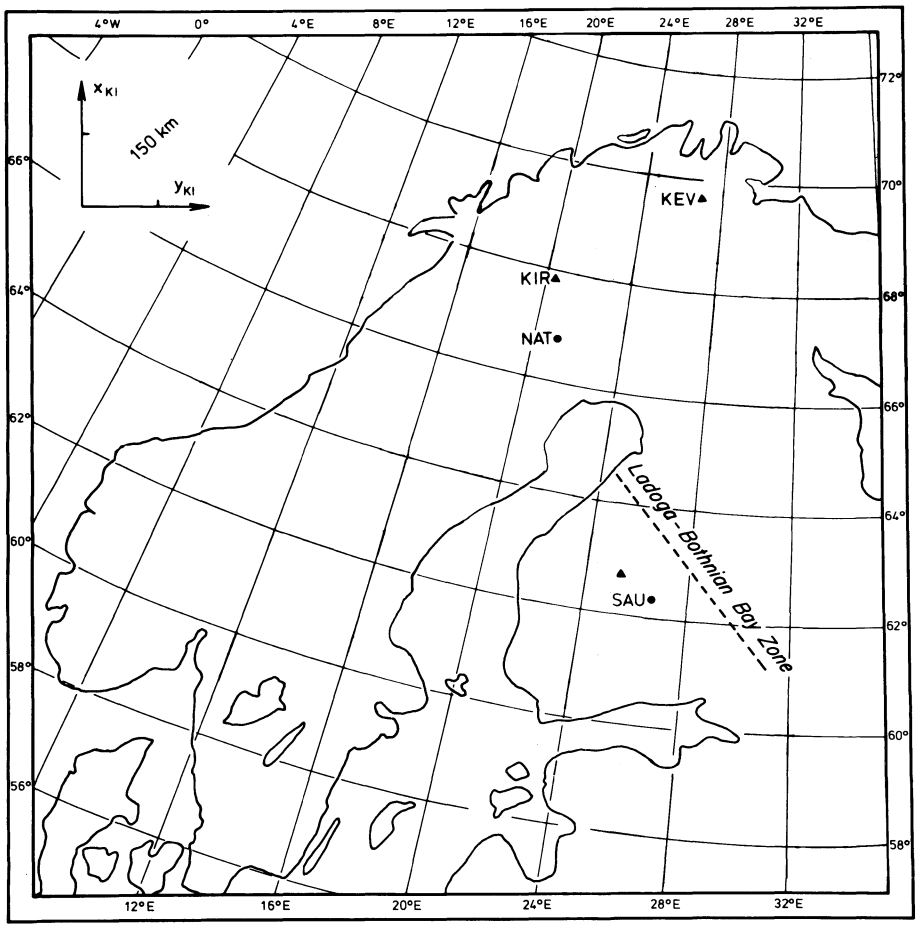

Fig. 1. Map showing the locations of the two sites at which magnetotelluric measurements were made (NAT and SAU *full circles*), together with the three locations at which HSG responses have been analysed (KIR, KEV and SAU *full triangles*). Also shown is the position of the Ladoga-Bothnian Bay zone

3. Observations

3.1 Nattavaara

The magnetotelluric observations at Nattavaara (NAT, see Fig. 1; for the co-ordinates see Table 1 of Küppers et al., 1979) were made during September, 1977. Ten events, totalling 56.5 h of data at 10 s digitizing interval, were chosen for analysis from the records by virtue of their signal content and differing polarizations of the magnetic field. The events were all of moderate activity, both to reduce, as much as possible, non-linear source field effects on the MT impedance tensor elements, **Z**, and to ensure that the telluric data remained within the dynamic range of the writers. Five of the events occured around local magnetic midday (approximately 10:35 UT, Whalen, 1970), two during the early evening hours (i.e., prior to the passage of the Harang discontinuity), and the remaining three during the early morning hours (i.e., shortly after the passage of the Harang discontinuity). No systematic variation in the derived elements of **Z** was observed for these three groups of data.

3.2 Sauvamäki

Magnetotelluric observations at Sauvamäki (SAU, see Fig. 1) were undertaken during June, 1979. The telluric recordings were not made at exactly the same location as the magnetometer, due to interference in the natural telluric field by the STARE radar of Greenwald et al. (1978), but at a site some 3 km from the magnetometer. A total of seven events, totalling 34.5 h of data at 10 s digitizing interval, were chosen for analysis, using the same criteria as described above, of which three included variations observed at local magnetic midnight (approximately 22:10 UT). Inspection of the induction vectors for these three indicated, however, that non-uniform source field effects were not apparent (see below). The telluric data for all seven events were recorded with the writers operating at the faster speed of 30 cm/h, i.e., 6 s/mm.

As discussed by several authors (Lilley, 1975; Beamish, 1980; Mareschal, 1981), non-uniform source fields have a far greater influence on the vertical to horizontal magnetic field ratio than on the MT impedance tensor, **Z**, or on the inductive transfer function, *C*. Hence, non-uniform source fields are more apparent in the derived induction vector responses than in the estimates of **Z**. An inspection of the induction vectors for all seven events illustrated that, in the period range 100–1,000 s, they were fully compatible with those derived for a uniform source field (see Paper II) at the 0.05 significance level (i.e., for 95% confidence).

AMT measurements were made at three locations within 4 km of the magnetometer and telluric sites during July, 1980. At each location, an attempt was made to discover any possible departures from a 1*D* earth by physically re-aligning the telluric spread at four different azimuths, namely 0°, 45°, 90°, and 135°, to local magnetic north. For each frequency, the final apparent

resistivity was determined by taking the geometric mean of five readings that were within a reasonable tolerance of each other. The geometric mean was taken, rather than the arithmetic mean, to be in accord with the notion that apparent resistivity displays a log-normal distribution (Bentley, 1973; Fournier and Febrer, 1976). A "regional" apparent resistivity curve was obtained by taking the geometric mean of all readings from the three locations and for all four orientations (see Fig. 9).

4. MT data analysis

4.1 General considerations

The analysis of MT data by techniques of statistical frequency analysis is open to many options and variants, and unfortunately not all authors explicitly details, or even state, the techniques that they have used. Whilst most of the methods employed on the data discussed herein can be considered as "standard practice", it is precisely because no "standard" yet exists in MT studies that a brief résumé is considered necessary.

Pre-processing of each data series included either trend removal (removal of a Lagrangian second-order interpolating polynomial, Jeffrey, 1971, pp. 336–337) or high-pass filtering (by two pole recursion filters, see Shanks, 1967), cosine tapering of the first and last 10% of the series (Bingham et al., 1967), and augmentation by zeroes to the next power of 2. It should be kept in mind that extension by zeroes implicitly increases the variance associated with each Fourier harmonic. If the data series are of required length, then the resulting complex Fourier harmonics will each have two degrees of freedom (one for each of the sine and cosine coefficients respectively), with the exceptions of the zero frequency (DC) and Nyquist frequency harmonics which are purely real and accordingly have only one degree of freedom. Hence, the variance associated with each Fourier harmonic estimate is as large as the estimate itself. Increasing the point length from, for example, M to M' by zeroes will reduce the number of degrees of freedom from 2 to $2M/M'$ (Bendat and Piersol, 1971, pp. 324–325) and simultaneously increases the variance by M'/M. Hence, unnecessary augmentation is to be strictly avoided.

After pre-processing, each data series was fast Fourier transformed, and the Fourier spectra were corrected for instrument response by Eqs. (1) and (2) above.

The raw spectra were then multiplied with the complex conjugate of each of the others to give the raw auto- and cross-spectra (henceforth "auto- and cross-spectra" will be referred to as simply "cross-spectra"), which were then frequency band averaged by spectral windows of constant-Q with a box-car form. From this smoothed auto- and cross-spectral matrix, or simply "spectral matrix", the timing discrepancies were estimated, and the relevant corrections made to the phases (see Sect. 4.4). The following parameters were then derived from the corrected spectral matrix:

(a) the polarization parameters of the horizontal magnetic and telluric fields (after Fowler et al., 1967),

(b) the bias-reduced ordinary, multiple and partial coherence functions between the various components (c.f. Sect. 4.5 below),

and

(c) the magnetotelluric impedance tensor elements, both unrotated and rotated.

The impedance tensor elements were estimated by two different approaches, and a third estimate was given by a weighted average of these two. The three estimates for, for example, the Z_{xy} tensor element were given by the following forms

$$\hat{Z}_{xy}=\frac{\hat{S}_{11}\hat{S}_{23}-\hat{S}_{21}\hat{S}_{13}}{\hat{S}_{11}\hat{S}_{22}-\hat{S}_{12}\hat{S}_{21}}, \tag{3.1}$$

$$\hat{Q}_{xy}=\frac{-\hat{A}_{xy}}{\hat{A}_{xx}\hat{A}_{yy}-\hat{A}_{xy}\hat{A}_{yx}}, \tag{3.2}$$

$$\hat{W}_{xy}=\frac{\hat{\gamma}^2_{32.1}\hat{Z}_{xy}+\hat{\gamma}^2_{23.4}\hat{Q}_{xy}}{\hat{\gamma}^2_{32.1}+\hat{\gamma}^2_{23.4}}, \tag{3.3}$$

where, for example, $\hat{S}_{12}$ is the estimated cross-spectrum between the H and D components, A_{xy} is the estimated admittance tensor element (see below), and $\hat{\gamma}^2_{32.1}$ is the estimated partial coherence between N and D with the influence of H on N removed in a least-squares manner.

The first form, $\hat{Z}_{xy}$, derived directly from the impedance tensor $\mathbf{Z}$ given by

$$\mathbf{E}(\omega)=\mathbf{Z}(\omega)\,\mathbf{H}(\omega), \tag{4}$$

is that most often employed in MT studies (for example, Swift, 1967; Vozoff, 1972; Reddy and Rankin, 1972; Kurtz and Garland, 1976; Rooney and Hutton, 1977; Jones and Hutton, 1979a), and is well-known to be *downward-biased* for any uncorrelated random noise contributions on the magnetic field, but unbiased for any uncorrelated noise on the telluric field (see, for example, Sims and Bostick, 1969; Sims et al., 1971).

The second form, $\hat{Q}_{xy}$, is derived from the admittance tensor $\mathbf{A}$, where

$$\mathbf{H}(\omega)=\mathbf{A}(\omega)\,\mathbf{E}(\omega) \quad \text{and} \quad \mathbf{Q}(\omega)=\mathbf{A}(\omega)^{-1} \tag{5}$$

and has been used recently by Chave et al. (1981), Cox et al. (1980) and Filloux (1980). This form is *upward-biased* for any uncorrelated noise contributions on the telluric data, but unbiased by uncorrelated noise on the magnetic data. However, it must be noted that the denominator of $\hat{A}_{xy}$ in Eq. (3.2) contains a multiplicative term which can be written as $(1-\hat{\gamma}^2_{34})$, indicating that the solution becomes unstable, and even indeterminable, when the telluric field is highly linearly polarized, as is often the case.

The third form, $\hat{W}_{xy}$, is a weighted average of the other two. Cox et al. (1980) and Chave et al., (1981) interpreted their two estimates, as given by the impedance and admittance tensors, Eqs. (4) and (5) above, independently, but this has little justification.

4.2 Frequency-time analysis

Due to decreasing signal-to-noise ratios at short periods, i.e., <200 s, many data sets did not give acceptable estimates of the impedance and/or admittance ten-

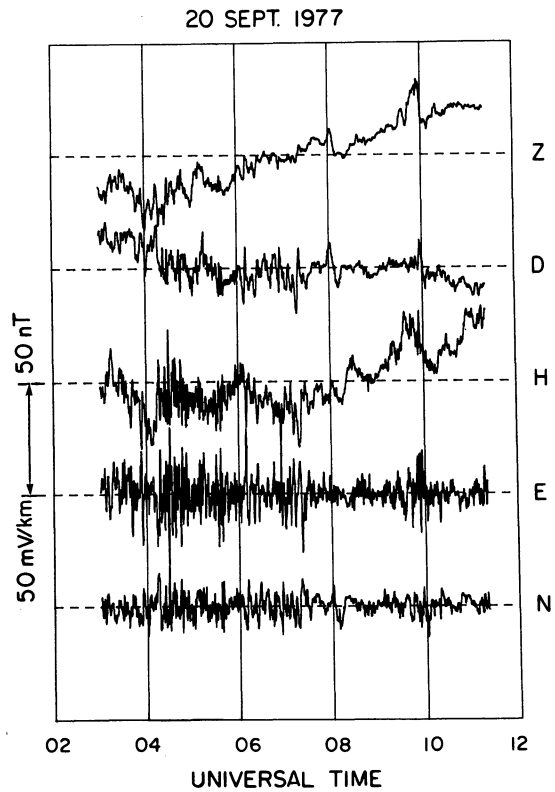

Fig. 2. A typical event of five components recorded at NAT

sor elements at these periods (see Sect. 4.6 for a discussion of the acceptance criteria employed). Hence, a frequency-time ($f-t$) analysis of all the events was undertaken. The form of the $f-t$ analysis has been described in full in Jones (1977), and briefly in Jones and Hutton (1979a), and is based on a procedure initially proposed by Welch (1967).

Every series of, say, M points was spliced into sub-series of length L points with L' points overlap, giving $(M/(L-L'))-1$ such sub-series. Each sub-series was then pre-processed and subsequently processed as detailed above, with the exception that a $1-|t|$ data window was applied rather than cosine belling, and certain parameters were calculated, from the ensembled sub-spectral matrices, and contoured. The sub-series exhibiting the desired characteristics were then picked out, and their cross-spectra were averaged to give the final spectral matrix for the short period data of the particular data set under consideration.

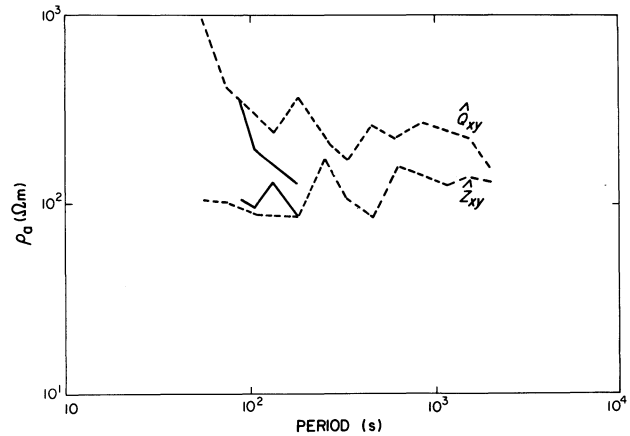

Fig. 3. The estimates of $\hat{Z}_{xy}$ and $\hat{Q}_{xy}$ from an analysis of the whole data set illustrated in Fig. 2 (*dashed lines*) and those from a selected sub-set of the event (*full lines*)

For example, for the 5-component data set of 30,000 s length (i.e., 3,000 points with 10 s digitization) illustrated in Fig. 2 (an event recorded at NAT), a "normal" analysis of the data gave the $\hat{Z}_{xy}$ and $\hat{Q}_{xy}$ estimates illustrated in Fig. 3. It is obvious, from their discrepancy, that the estimates appear to have large bias errors at short periods. As shown in Figs. 4a and b, this increasing bias error is probably due to the decreasing signal-to-digitizing noise level with decreasing period. Undertaking an $f-t$ analysis of the data, with $L=256$, $L'=128$, and a Q factor of 0.2, gave 22 sub-data sets with 10 frequencies at which smoothed estimates were derived in each. Contouring the Normalized Transformed Partial Coherency (NTPC) functions $\hat{N}_{32.1}$ and $\hat{N}_{41.2}$ (Jones, 1981b) indicates that superior estimates can be obtained at short periods by selecting

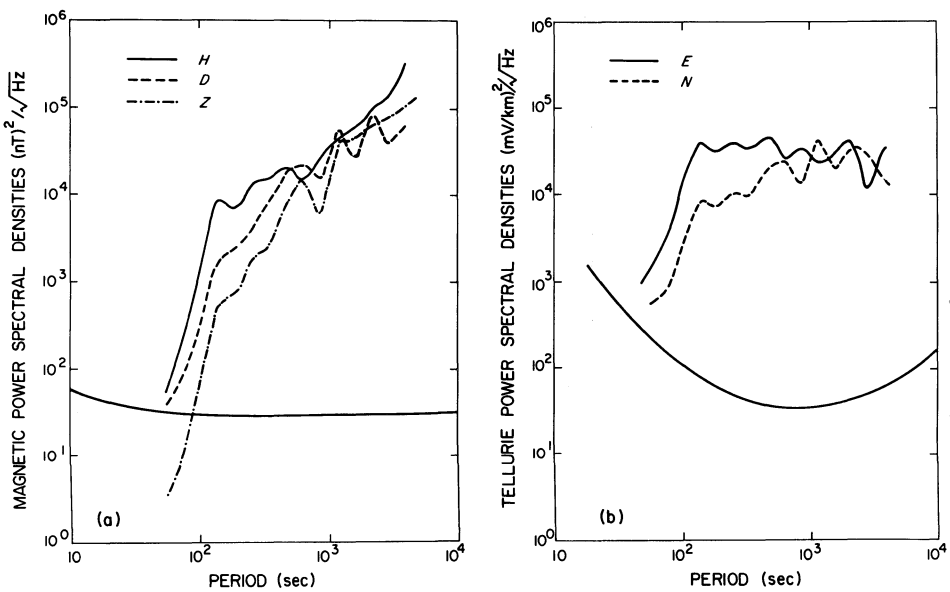

Fig. 4a and b. The auto power spectral densities of **a** the magnetic components and **b** the telluric components illustrated in Fig. 2. The *full line* along the lower part of the figure is the estimated noise power introduced by the manual digitizing of the records (note that it is not flat due to the frequency response of the instruments)

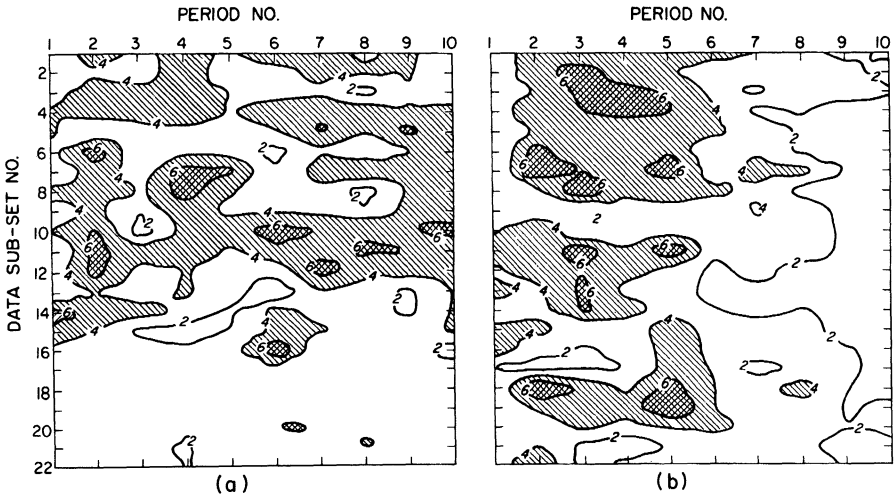

Fig. 5. a The contoured estimate of the Normalised Transformed Coherency Function between the north telluric component and the east magnetic component, with the effect of the north magnetic component removed in a least-squares sense ($\hat{N}_{32.1}$), in the frequency-time domain (frequency increasing from left to right-time increasing from top to bottom) **b** as for **a** but for the $\hat{N}_{41.2}$ estimate. The period numbers refer to the following periods: 1:1,280 s; 2:465 s; 3:270 s; 4:175 s; 5:130 s; 6:105 s; 7:90 s; 8:75 s; 9:60 s; 10:50 s

splices of the data than by employing the whole data sets (Figs. 5a and b).

These NTPC functions are defined, for example for $\hat{N}_{32.1}$, by

$$\hat{N}_{32.1} = \frac{\operatorname{arctanh}(|\hat{\gamma}_{32.1}|)}{\operatorname{arctanh}\left(\frac{(2\nu+4)^{1/2}}{\nu-2}\right)} \tag{6}$$

(Jones, 1977, 1981b), where the numerator is the positive square root of the estimate of the partial coherence $\hat{\gamma}^2_{32.1}$ transformed, by the Fisher z-transformation (see, for example, Hald, 1952, p. 609), into a domain in which it exhibits a more nearly normal distribution, and the denominator is the transformed expectation value of the estimate of the positive square root of the partial coherence when all three series are totally uncorrelated, ν being the number of degrees of freedom associated with the estimate. The variance of $\hat{N}_{32.1}$ is

$$\operatorname{Var}(\hat{N}_{32.1}) = \frac{\nu+2}{(\nu-2)^2 \operatorname{arctanh}\left(\frac{(2\nu+4)^{1/2}}{\nu-2}\right)} \tag{7}$$

(Jones, 1977, Eq. (4.66c), and these normalised transformed coherence functions have the property that $E[\hat{N}] = 1$ for totally uncorrelated series, thus indicating directly the coherent to incoherent signal ratio. The other properties that make these functions preferable to the usual coherence functions are given in Jones (1981b). Hence, for example for $\nu = 12$, values of $\hat{N}_{32.1}$ above 2.25 are indicative of a true correlation between N and D at the 95% confidence level (given by $1 + 1.96\,(\operatorname{Var}(\hat{N}))^{1/2}$).

From Figs. 5a and b, sub-series were chosen in which $\hat{N}_{32.1}$ or $\hat{N}_{41.2}$ was >6. Those selected were (for the definitions of the period numbers, see the caption to Fig. 5):

period no.	*sub-sets chosen*		
4		4	7
5	7	11	19
6	10	16	20
7	5	7	12

The resulting estimates of $\hat{Z}_{xy}$ and $\hat{Q}_{xy}$ from this selection are also illustrated in Fig. 3, where it can be seen that the estimates from this $f-t$ analysis display far smaller bias errors. (Note that the number of operations required to FFT a dataset of length M is $2M \log_2 M$. Hence, the number of operations required to FFT all spliced series is $(2L\log_2 L)((M/(L-L'))-1)$. Thus, for a data set of 4,096 points, an FFT of the total series requires 98,304 operations, whilst an $f-t$ analysis with $L=256$ and $L'=128$ requires 111,104 operations, hence entailing virtually the same CPU time, but giving far superior information at shorter periods.)

4.3 Analysis strategy for 1D data

Many workers analyse their data by the same algorithms, regardless of the nature of the location where the observations were made or of the structure of the data themselves. Such an approach can, in the opinion of the authors, lead to biased and incorrect models which are concluded as being indicative of the actual structure of the earth that gave rise to the estimated responses. Hence, below is presented an "analysis strategy" which, hopefully, will lead to far more reliable parameters for inversion of 1D data.

There are many signatures of data which indicate that the earth's conductivity structure beneath the recording location may be assumed to vary with depth alone in the period range of observation. The major indicators are (for uniform field events):

(1) low order of anisotropy between the two off-diagonal elements of the impedance tensor, $\hat{Z}_{xy}$ and $\hat{Z}_{yx}$,

(2) small values for the diagonal elements of the impedance tensor relative to the off-diagonal elements (i.e., small values of SKEW),

(3) no dominant maximising direction of the impedance tensor with frequency or with differing events,

(4) small, or zero, induction response functions ($\hat{\mathbf{A}}$, $\hat{\mathbf{B}}$), i.e., small induction vectors,

and

(5) no strong geological or tectonic boundaries close, in terms of inductive scale length; to the recording location, i.e., coastlines, major faults, subduction zones, volcanoes, major folds, mountain ranges, etc. (Here it is assumed that these boundaries give rise to a juxtapositioning of rocks of differing properties such that they are of differing electrical conductivity. If the

boundary is between rocks of the same electrical conductivity, then obviously no spatial variation in the electromagnetic fields due to the boundary will occur.)

If the data and the recording location display all these features, then it may be confidently assumed that a $1D$ model for the data will be valid – or, at the very least, defensible. For analysis of $1D$ data, the object should be to maximise the signal-to-noise ratio in one of the off-diagonal elements of the tensor under consideration (either impedance or admittance). As different events will display differing polarization characteristics, then the impedance and/or admittance tensor should be rotated into that direction which gives the maximum coherence between the telluric component of interest and its corresponding magnetic component. It is well-known that the ordinary coherence between, say, the N component and the D component, viz. γ^2_{32}, does not truely reflect their correlation due to the influence of the H component on N for the impedance tensor, or the E component on D for the admittance tensor. Hence, the coherence functions to employ are the *partial* coherences between either N and (H, D) for the impedance tensor, or D and (N, E) for the admittance tensor. Accordingly, the impedance tensor should be rotated into that direction in which $\hat{\gamma}^2_{32.1}$ displays a maximum, and the element $\hat{Z}'_{xy}$ (the prime denotes a rotated parameter or response) interpreted in a $1D$ sense. Similarly, the admittance tensor should be rotated into that direction in which $\hat{\gamma}^2_{23.4}$ displays a maximum, and element $\hat{Q}'_{xy}$ interpreted in a $1D$ sense. (The use of partial coherence functions in MT data analysis was first proposed by Reddy and Rankin (1974).)

Estimate $\hat{W}'_{xy}$, i.e., the coherence weighted average of $\hat{Z}'_{xy}$ and $\hat{Q}'_{xy}$ as given by Eq. (3.3), is considered to be the most suitable parameter for interpretation when it is believed that the noise contributions on the magnetic and telluric components are of approximately equal relative magnitude.

4.4 Timing error correction

For MT analysis, all that is usually required is that the relative timing between the magnetic and telluric components be as accurate as possible. However, for the instrumentation used in this study, accurate absolute timing was essential for reliable MT phase determination. The two recording instruments, magnetic and telluric, were operated independently, and, although the absolute timing for each was probably to better than 5 s, a cumulative error of 10 s was possible. Also, the telluric traces were of the order of 0.5 mm thick, hence on the slower speed of 12 s/mm a resolution error of up to 6 s was likely. Furthermore, problems were encountered with the internal clock of the telluric recorder which malfunctioned intermittently and occasionally did not produce the desired hour mark on the records. Linear interpolation was used between recognizable hour marks, but variations in temperature and humidity could have lead to non-constant chart drives.

Accordingly, timing errors as great as 20 s or so could be expected. Such a timing discrepancy between the telluric and magnetic data would cause an error in phase of 72° at 100 s period, reducing to 7.2° at 1,000 s period, which would make the short period, i.e., <500 s, phase data totally unreliable. Although the phase and apparent resistivity are not independent but are related by the Hilbert transform (see, for example, Weidelt, 1972; Fischer and Schnegg, 1980; Paper I), as shown by a number of workers (for example, Parker, 1970; Jones and Hutton, 1979b) the phase information provides an additional set of constraints on the acceptable model parameters that satisfy the observed response. Hence, it was considered worthwhile to try to recover the phase information by a scheme in which the linear dependence of a given phase on ω is reduced, by a regression technique, as much as possible. Also, reliable phase estimates are *essential* if the MT impedance and/or admittance tensors are to be rotated. It would have been possible to calculate Weidelt's (1972) "approximate phase" from the gradient of the apparent resistivity curve, but this is only an approximation and is not to be preferred over real data.

For two series, $x(t)$ and $y(t)$, which in the frequency domain are $X(\omega)$ and $Y(\omega)$, the cross-spectrum between them is given by $S_{xy}(\omega) = X^*(\omega)\, Y(\omega)$ (smoothing considerations are disregarded for this description). Should there be a timing error of d, such that the measured data are $x(t)$ and $y'(t)$, where $y'(t) = y(t+d)$, then the estimated cross-spectra will be $S'_{xy}(\omega) = X^*(\omega)\, Y'(\omega)$, where $Y'(\omega) = Y(\omega) \exp(i\omega d)$. Hence, $S'_{xy}(\omega) = S_{xy} \exp(i\omega d)$, and the phases are related by $\phi'_{xy}(\omega) = \phi_{xy}(\omega) + \omega d$. Thus, the phase estimates of the cross-spectrum $S'_{xy}(\omega)$ will display a *linear dependence* on ω. Accordingly, an estimate of the timing error d may possibly be obtained by a linear regression of the phase of $S'_{xy}(\omega)$ on ω. This estimate is given by

$$\hat{d} = \frac{m \sum_{\omega_1}^{\omega_2} \omega \phi'_{xy}(\omega) - \sum_{\omega_1}^{\omega_2} \omega \sum_{\omega_1}^{\omega_2} \phi'_{xy}(\omega)}{m \sum_{\omega_1}^{\omega_2} \omega^2 - \left(\sum_{\omega_1}^{\omega_2} \omega \right)^2} \tag{8}$$

where the error is estimated in the frequency range (ω_1, ω_2), and there are m estimates of $S'_{xy}(\omega)$ in that range. The frequency range should be as large as possible so that any real dependency of $S_{xy}(\omega)$ on ω is as small as possible.

For MT data, there are a number of choices of which phase to use in order best to determine d. The phase of, for example, S_{32} is equivalent to the phase of the complex ordinary coherency between N and D,

$$\gamma_{32} = \frac{S_{32}}{(S_{33} S_{22})^{1/2}}.$$

(Note the terminology throughout – any frequency domain measure of correlation which is a modulus squared quantity is termed a "coherence", and its plural is "coherences". The unsquared quantities, which may be complex, are termed "coherency" and "coherencies" respectively.) However, the linear system represented by the MT impedance or admittance tensors is a two-input/two-output system, and hence ordinary coherences (and accordingly complex ordinary coherencies) do not give a true estimate of the correlation between the two components of interest due to other inputs and outputs on the system. For such data, the correct phase to use is the phase of the complex *partial* coherency between, for example, N and D, $\gamma_{32.1}$, which is equal to the phase of the impedance tensor element Z_{xy}.

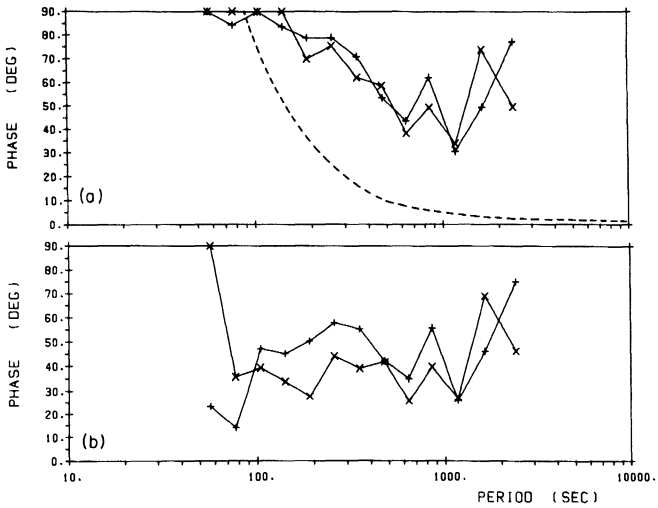

Fig. 6. a The phase of the estimates of the off-diagonal impedance tensor elements ($\hat{Z}_{xy}$ shown as $\times$, and $\hat{Z}_{yx}$ as $+$) before the timing correction was applied. The *dashed line* is an illustration of the additive effect on the phase for a timing discrepancy of 22 s **b** as for **a** but after correction for timing discrepancy between the telluric components and the magnetic ones

The N and E telluric components were recorded on separate chart recorders (but using the same clock), and were digitized seperately, hence there was no reason to assume that the timing errors between N and (H, D), and E and (H, D), were exactly equal. Accordingly, two different timing corrections were derived, d_n and d_e, from the phases of the uncorrected preliminary estimates of the Z_{xy} and Z_{yz} tensor elements respectively. These timing errors were calculated from the phase responses in the period range 50–1,000 s, i.e., over one and one-half decades.

As an example of the application of the above described timing error corrrection method, Figs. 6a and b display the phases of $\hat{Z}_{xy}$ and $\hat{Z}_{yx}$ for an event observed at SAU. The uncorrected original estimates of the phases show physically unreasonable values towards the shorter periods, whilst the corrected phases are within the bounds 0°–90°, and agree with each other (which is to be expected as SAU is considered a 1D location in the period range of interest considered herein). The estimated timing errors for the two telluric components are -23.1 s for the N component and -21.6 s for the E component, which are of the expected order of magnitude, and are approximately equal (due to the common clock). Also shown on Fig. 6a is the additive effect on the phase due to a timing discrepancy of 22 s.

Two other recent investigations have attempted to correct possible timing discrepancies between the electric and magnetic components by investigating the dependency of a certain phase on ω (Cox et al., 1980; Chave et al., 1981). Both, however, used the phase of the complex ordinary coherency, which, as discussed above, is not considered to be the correct choice. Also, Cox et al. (1980) assumed that the phase lead of E relative to H at frequencies close to 10 cph should be $\pi/4$. Such a restrictive assumption is not made in the procedure described above.

4.5 Bias-reduced coherence functions

The normalized transformed coherence functions (Jones, 1977, 1981b and Sect. 4.2 herein) have not received widespread use, possibly due to the fact that they are defined in the range $[1, \infty]$, rather than the common coherence functions which are defined in the range $[0, 1]$. Hence, *bias-reduced* coherence functions are defined here.

It is relatively well-known that the estimates of the various coherence functions are biased, i.e., when all the components involved are totally uncorrelated the estimated coherence functions are non-zero. For the case of totally uncorrelated series, the biases of the estimates of the ordinary, multiple and partial coherence functions are given by

$$B(\hat{\gamma}^2_{xy}, 0) = \frac{2}{\nu}, \tag{9.1}$$

$$B(\hat{\gamma}^2_{zxy}, 0) = \frac{4}{\nu - 2}, \tag{9.2}$$

$$B(\hat{\gamma}^2_{zx\cdot y}, 0) = \frac{2\nu + 4}{(\nu - 2)^2} \tag{9.3}$$

(Jones, 1977), where ν is the number of degrees of freedom associated with the estimate. When the true coherences are non-zero however, these biases are reduced. Assuming that there is no bias due to misalignment (Carter, 1980), which should be the case as the series have been aligned as described in the previous section, Nuttall and Carter, (1976) have shown that the bias of the estimate of the ordinary coherence function is given by

$$B(\hat{\gamma}^2_{xy}, \gamma^2_{xy}) = B(\hat{\gamma}^2_{xy}, 0)\,(1 - \gamma^2_{xy})^2\,(1 + 4\gamma^2_{xy}/\nu) \tag{10}$$

where γ^2_{xy} is the true ordinary coherence. An estimate of this bias can be obtained from

$$\hat{B}(\hat{\gamma}^2_{xy}, \gamma^2_{xy}) = \frac{2}{\nu}(1 - \hat{\gamma}^2_{xy})^2\,(1 + 4\hat{\gamma}^2_{xy}/\nu) \tag{11}$$

and accordingly a bias-reduced estimate of the ordinary coherence can be defined by

$$(\hat{\gamma}^2_{xy})_b = \hat{\gamma}^2_{xy} - \hat{B}(\hat{\gamma}^2_{xy}, \gamma^2_{xy}). \tag{12}$$

As the estimates of the multiple and partial coherence functions have the same distribution functions as those of the ordinary coherence function, estimates of the bias-reduced forms of these functions are given by

$$\begin{aligned}(\hat{\gamma}^2_{zxy})_b &= \hat{\gamma}^2_{zxy} - \hat{B}(\hat{\gamma}^2_{zxy}, \gamma^2_{zxy}) \\ &= \hat{\gamma}^2_{zxy} - \left(\frac{4}{\nu - 2}\right)(1 - \hat{\gamma}^2_{zxy})^2(1 + 4\hat{\gamma}^2_{zxy}/\nu)\end{aligned} \tag{13}$$

and

$$\begin{aligned}(\hat{\gamma}^2_{zx\cdot y})_b &= \hat{\gamma}^2_{zx\cdot y} - \hat{B}(\hat{\gamma}^2_{zx\cdot y}, \gamma^2_{zx\cdot y}) \\ &= \hat{\gamma}^2_{zx\cdot y} - \left(\frac{2\nu + 4}{(\nu - 2)^2}\right)(1 - \hat{\gamma}^2_{zx\cdot y})^2(1 + 4\hat{\gamma}^2_{zx\cdot y}/\nu).\end{aligned} \tag{14}$$

4.6 Averaging procedures and acceptance criteria

The most usual method for deriving an estimate of a response function (or functions) from a number of realizations is to average the raw, or unsmoothed, cross-spectra for all the available data and to derive the

estimates of the function from the averaged spectral matrix. The confidence intervals could then be derived from the expression given in Goodman (1965, repeated in Bendat and Piersol, 1971, pp. 199–203). This approach, however, could lead to domination of the spectral matrix by certain realizations with high power levels, and the confidence limit estimation requires that the noise components be normally distributed. An alternative approach is to average together, in a weighted manner, the estimated response functions from each realization, and to derive the confidence intervals by utilising the Student-t distribution. The latter procedure assumes merely that the Central Limit Theory is valid for the data. Even if the distributions of the components in the time domain are not Gaussian, i.e., not normal, the distributions in the frequency domain should certainly approach the normal form, and the distributions of the means of the components, which is equivalent to the smoothed estimates of the response functions, will be normal.

Accordingly, the response functions $\hat{\mathbf{Z}}$, $\hat{\mathbf{Q}}$ and $\hat{\mathbf{W}}$, from each realization could have been averaged together, to obtain the final estimates, by expressions of the form

$$\bar{Z}_{xy} = \frac{\sum_{i=1}^{m} w_i \hat{Z}_{xy}}{\sum_{i=1}^{m} w_i} \tag{15}$$

where m was the number of available estimates, and w_i was the weighting factor for the i'th estimate. However, due to the aforementioned problem regarding reliable phase determination, the apparent resistivity and phase estimates were averaged independently from each other by expressions similar to Eq. (15), where the weighted average of apparent resistivity was derived on a logarithmic scale due to its lognormal, rather than normal, distribution (Bentley, 1973; Fournier and Febrer, 1976). The weights chosen were the bias-reduced estimates of the partial coherences, viz. $(\hat{\gamma}^2_{32.1})_b$ and $(\hat{\gamma}^2_{23.4})_b$, for the impedance and admittance estimates respectively.

The above defined bias-reduced partial coherences were employed not only as weights, but also as acceptance criteria for the estimates of the tensor elements. The estimate of the bias-reduced partial coherence had to be greater than 0.8 for acceptance. As the partial coherence functions are always less than the multiple coherence functions, this acceptance criterion, it should be noted, is stricter than one of $\hat{\gamma}^2_{312} > 0.8$ employed, for example, by Swift (1967), Kurtz and Garland (1976) and Rooney and Hutton (1977). Also, because the *bias-reduced* forms are used, the acceptance criterion is probably stricter than $\hat{\gamma}^2_{312} > 0.9$ as used by Reddy and Rankin (1972), Vozoff (1972) and Reddy et al. (1976).

5. Results

5.1 Nattavaara

An inspection of the data recorded at NAT showed that, for all events, the two unrotated off-diagonal tensor elements lay within the bias errors of each other, and the diagonal elements were all 10% or less of the off-diagonal elements. Also, the direction in which the

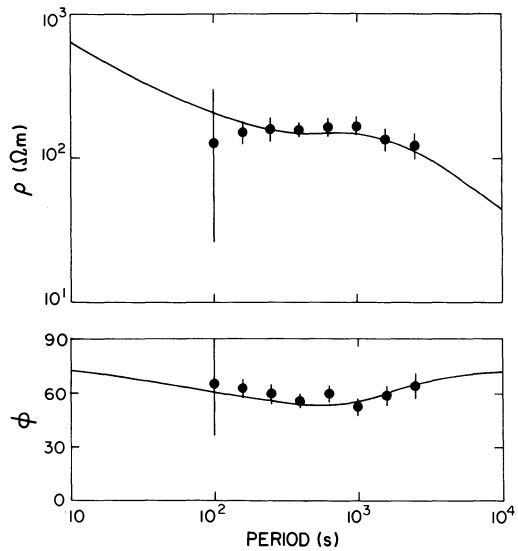

Fig. 7. The final averaged estimates of $\hat{W}'_{xy}$ for NAT, with standard errors on the $\hat{W}'_{xy}$ responses. The *full line* is the theoretical response of the best-fitting model (listed in Table 2a) discovered by the search procedure

partial coherence function $(\hat{\gamma}^2_{31.2})_b$ displayed a maximum appeared to be random, i.e., no consistent direction was apparent over the whole frequency range and over all seven events analysed. Both the real and imaginary induction vectors for a uniform field event were <0.2 in the period range 100 s–1,000 s (Paper II, Figs. 10a–d and 11a–d). Nattavaara is in the same tectonic setting as Kiruna (KIR, Fig. 1), and HSG data centred on KIR were shown in Papers I and Ib to be fully compatible with a 1D interpretation. Hence, all four facts indicate that the data may be interpreted in a 1D manner, and accordingly the data were analysed as described in Sect. 4.3.

The final estimates of W'_{xy}, are illustrated in Fig. 7 in terms of apparent resistivity and phase. The limits shown on the estimates are standard errors, i.e., the 68% confidence intervals. The averaged estimates of $\hat{Z}'_{xy}$ and $\hat{Q}'_{xy}$ displayed downward and upward biasing respectively, due to the noise contributions on the magnetic and telluric fields. The bias errors however, estimated by $(\hat{Q}'_{xy} - \hat{Z}'_{xy})/2$, were of the same order of magnitude as the random errors. The estimated response function $\hat{W}'_{xy}$ was taken as indicative of the conductivity-depth structure beneath NAT. This function was tested for validity by the nine inequalities given by Weidelt (1972, reproduced in Paper I). Of the 72 inequalities (9 at each of 6 periods), only 4 were not upheld, thus giving greater confidence to the belief that the NAT response may be interpreted in a 1D manner. The NAT responses are listed in Table 1a.

In Jones (in press 1983b), the NAT response is compared with that from the HSG analysis of data centred on KIR (see Fig. 1). For the two techniques, MT and HSG, a different character of the source field is required. In order to interpret single-station MT responses (i.e., when there is no knowledge of the source structure), the source must be either uniform, or have a linear dependence with horizontal distance (Dmitriev and Berdichevsky, 1979; Schmucker, 1980). For HSG

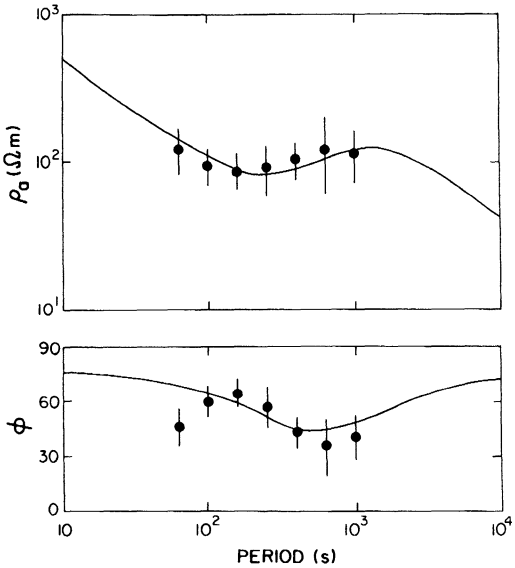

Fig. 8. The final averaged estimates of $\hat{W}'_{xy}$ for SAU, with standard errors on the $\hat{W}'_{xy}$ responses. The *full line* is the theoretical response of the best-fitting model (listed in Table 2) discovered by the search procedure

data however, the source must be sufficiently non-uniform that the gradients of the horizontal magnetic field with lateral distance can be reliably estimated. Notwithstanding these basic requirements of the data, the inductive response functions observed at KIR and NAT are in total accord with one another. This fact indicates that not only have the timing error corrections been performed satisfactorily, but also that there are no appreciable telluric distortion effects, of the form described by Richards et al. (1982), or current channelling phenomena (see Jones, in press 1983c for a review of this highly contentious subject), occuring in northern Sweden.

Also in Jones, (1983b), the χ^2 misfit of the D^+ model, found by Parker's (1980) scheme, to the NAT response is derived. This misfit is 3.62, which implies that there is very little confidence in accepting the hypothesis that the data do not originate from a $1D$ earth.

5.2 Sauvamäki

As with the NAT responses, the unrotated off-diagonal impedance tensor estimates ($\hat{Z}_{xy}$ and $\hat{Z}_{yx}$), and the off-diagonal inverse admittance tensor estimates ($\hat{Q}_{xy}$ and $\hat{Q}_{yx}$), were all within the statistical bounds (at 68%) of each other. Also, the real and imaginary induction vectors observed at SAU for a uniform field event were all less than 0.2 in the period range 10^2–10^3 s (Paper II, Figs. 10a–d and 11a–d). The nearest known large geological feature to the site is the Lake Ladoga-Bothnian Bay zone (LBBZ), or Svecokarelian fault, lying approximately 60 km to the NE (see Fig. 1). Hence, it was considered justifiable to analyse and interpret the data in a $1D$ manner (see Sect. 7 for a further examination of this point).

The final estimates of W'_{xy} are illustrated in Fig. 8 in terms of apparent resistivity and phase, with standard errors as shown. These estimates were also tested for

Table 1a. Estimated response function for NAT with associated standard errors (i.e., 68% confidence)

Period (s)	ρ_a (Ωm)	ϕ (degrees)	ρ_a+se (Ωm)	ρ_a-se[a] (Ωm)	$\phi+se$ (degrees)	$\phi-se$ (degrees)
100	127	65.3	303	26.3	90.0	36.7
160	150	62.7	179	124	67.8	57.5
250	158	59.7	193	127	65.7	53.8
400	156	55.6	171	141	58.2	52.9
630	160	59.6	186	135	64.1	55.1
1,000	165	52.3	192	141	56.7	48.0
1,600	135	58.7	161	110	64.1	53.3
2,500	119	63.8	147	94.7	70.1	57.6

Table 1b. Estimated response function for SAU with associated standard errors (i.e., 68% confidence)

Period (s)	ρ_a (Ωm)	ϕ (degrees)	ρ_a+se (Ωm)	ρ_a-se (Ωm)	$\phi+se$ (degrees)	$\phi-se$ (degrees)
63	119	46.2	116	80.5	56.3	36.0
100	93.7	59.8	122	69.1	67.8	51.7
160	85.3	63.8	106	66.6	70.4	57.2
250	91.8	56.8	132	58.4	68.2	45.3
400	103	43.6	137	74.3	52.2	34.9
630	121	36.0	203	60.0	52.4	19.6
1,000	112	40.4	165	70.1	52.3	28.5

[a] se = standard error

validity by Weidelt's inequalities. Of the 63 inequalities (9 at each of 7 periods), 21 were violated, principally at the shortest and longest periods but also due to the minimum in the real part of the response function, $\hat{g}_{SAU}$, when it is expressed as Schmucker's inductive response function, $C(\omega)$, at 630 s (see Jones, 1983b, Fig. 2). Smoothing the real and imaginary parts of the response function independently with a 3 point Hanning window, $(\frac{1}{4}, \frac{1}{2}, \frac{1}{4})$, yielded a response function of which only 14 estimates violated the inequalities. These smoothed data are listed in Table 1b. The main cause for the violation of these 14 inequalities was the badly estimated phase response at the shortest period. It was therefore concluded that the timing error correction had not completely removed the effects due to incorrect timing, and hence the shortest period phase response was ignored in the Monte-Carlo model search procedure, which is discussed below.

The SAU MT response is compared with the HSG one for the region in Jones (1983b). The two are shown to be highly compatible, and hence the above comments about the northern Sweden region, regarding the lack of telluric distortion effects and/or current channelling phenomena, are also valid for the locale around SAU. This fact is considered further, in the comparison with the results of other MT studies conducted in Finland, in the Discussion. The χ^2 misfit of the SAU response to the D^+ model is 9.67, which gives little confidence in the hypothesis that the data do not originate from a $1D$ earth.

Illustrated in Fig. 9 are the AMT apparent resistivity geometric means, together with their sample standard deviations. Apart from the highest frequency estimate (at 3,700 Hz), the response describes a uniformly

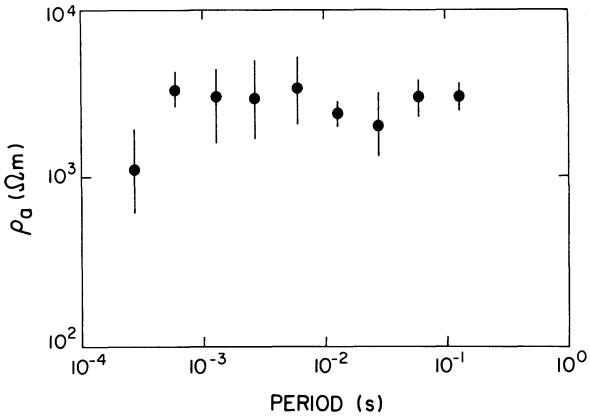

Fig. 9. The locally-averaged AMT apparent resistivities, with associated sample standard deviations, for the three stations close to SAU

resistive top layer of some 3,000 Ωm. The skin depth at the lowest frequency (8 Hz) is of the order of 10 km, implying that the uppermost layer is of 10 km minimum thickness. The AMT data were used only in a qualitative manner, to constrain the topmost layer parameters, in the Monte-Carlo inversions.

6. Models

6.1 First-approximation continuous models

To gain an initial impression of the conductivity-depth structure beneath the MT recording locations, a modified form of the Niblett-Bostick (Niblett and Sayn-Wittgenstein, 1960; Bostick, 1977; see also Weidelt et al., 1980 and Jones, 1983a) transformation was employed. The Niblett-Bostick transformation gives a resistivity ρ_B at depth h, from the apparent resistivity curve alone, from

$$h=\left(\frac{\rho_a(T)\,T}{2\pi\mu_0}\right)^{1/2} \tag{15}$$

and

$$\rho_B(h)=\rho_a(T)\left(\frac{1+m(T)}{1-m(T)}\right) \tag{16}$$

where

$$m(T)=\frac{d\log(\rho_a(T))}{d\log(T)}. \tag{17}$$

The Niblett-Bostick transform is known to perform well in the case of a decrease in resistivity with depth, but not so well for an increase of resistivity with depth. This is due to the reluctance of current to enter a more resistive layer. In order to compensate partially for this effect, the gradient of $m(T)$ is taken into consideration, i.e.,

$$m'(T)=\frac{d^2\log(\rho_a(T))}{d^2\log(T)}. \tag{18}$$

If both $m(T)$ and $m'(T)$ are positive, then the apparent resistivity curve indicates that, at the periods of interest, a transition is being made between a less resistive layer and an underlying more resistive one. Conversely, if both $m(T)$ and $m'(T)$ are negative, then the opposite is true. Hence, a first-order inversion is defined by resistivity ρ_J, at depth h, given by

$$\begin{aligned}\rho_J(h)&=\rho_a(T)\left(\frac{1+m(T)}{1-m(T)}\right)\\ &\quad\text{for } \operatorname{sign}(m)\neq\operatorname{sign}(m'),\\ \rho_J(h)&=\rho_a(T)\left(\frac{1+\operatorname{sign}(m)\,(|m|)^q}{1-\operatorname{sign}(m)\,(|m|)^q}\right)\\ &\quad\text{for } \operatorname{sign}(m)=\operatorname{sign}(m')\end{aligned} \tag{19}$$

where

$$q=\begin{cases}1/(1+m)^2 & \text{for } m(T)>0\\ 1/(1-m)^{1/2} & \text{for } m(T)<0.\end{cases} \tag{20}$$

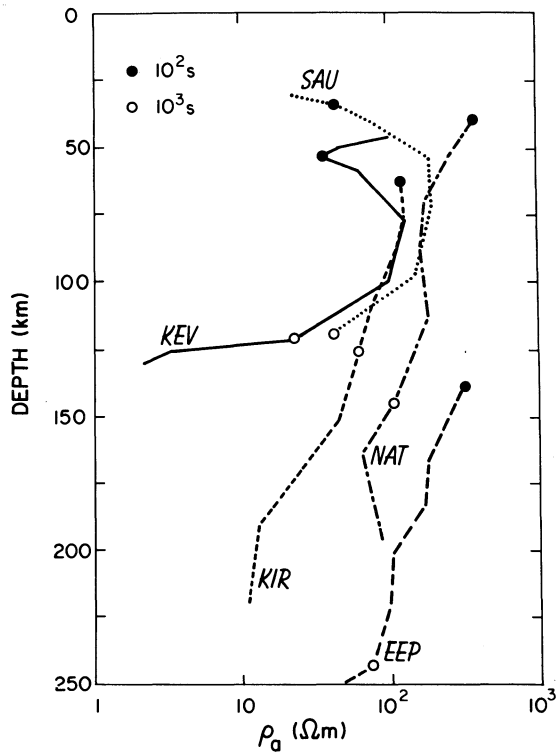

Fig. 10. The modified Niblett-Bostick first-approximation continuous models for the MT stations NAT and SAU. Also shown are the models for KIR and KEV (see Fig. 1) from their HSG responses, and for the East European Platform (EEP)

Figure 10 shows the modified Niblett-Bostick transformations of the two MT response functions, together with those of the inductive response functions, $C(\omega)$, estimated by the HSG method for northern Sweden (KIR) and northwestern Norway/northern Finland (KEV) (Papers I, Ib), and of the generalised curve for the East European Platform (EEP), as presented by Vanyan et al. (1977). The transformation of the HSG response observed at SAU is not included due to the lack of confidence in the imaginary part, i.e., $\hat{h}_{\mathrm{SAU}}$. These transformations indicate that the upper mantle beneath Scandinavia is remarkably similar everywhere, of resistivity around 100 Ωm. This value is more than an order of magnitude smaller than that of the "normal geoelectric profile" for the EEP at similar depths (Vanyan et al., 1977, 1980).

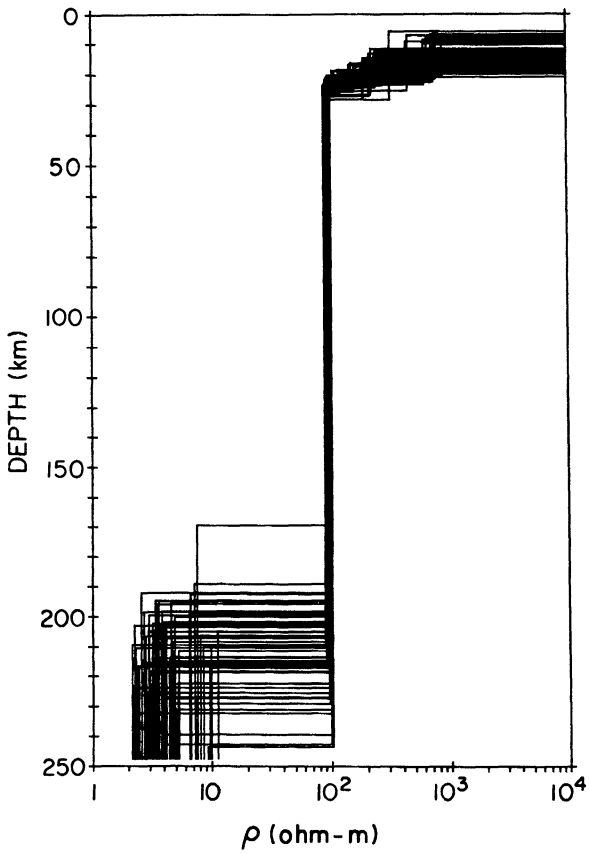

Fig. 11. The resistivity-depth profiles of models found that are acceptable to the NAT response illustrated in Fig. 7

Table 2a. Statistics of the acceptable model parameters to the NAT response

Layer	Mean	Min	Max	Mean $-Sd$[a]	Mean $+Sd$	Best
			Layer resistivities (Ωm)			
1	10,000	–	–	–	–	10,000
2	284	106	895	150	540	123
3	96	89	101	93	99	95
4	4.1	2.1	11.3	2.6	6.3	4.2
			Layer depths (km)			
1	13.6	5.7	20.8	9.7	19.1	18.6
2	22.8	20.2	28.3	20.8	24.9	25.7
3	211	170	244	197	225	201

Table 2b. Statistics of the acceptable model parameters to the SAU response

Layer	Mean	Min	Max	Mean $-Sd$	Mean $+Sd$	Best
			Layer resistivities (Ωm)			
1	3,000	–	–	–	–	3,000
2	25.3	12.1	51.3	17.5	36.5	42.9
3	161	63.2	477	93.3	278	327
4	5.3	2.0	11.7	3.1	9.1	2.8
			Layer depths (km)			
1	22.5	15.5	29.0	19.5	25.9	19.8
2	42.2	27.9	59.1	35.2	50.7	58.7
3	188	153	248	166	213	201

[a] Sd = Standard deviation of the sample

The other features of note are *(i)* that the KIR and NAT transformations are very similar, and *(ii)* that the SAU transformation indicates the existence of a lower crustal conductor. There is the indication from the KEV transformation of a conducting zone beneath northeastern Norway/northern Finland. This feature was not confirmed however in the model searches described in Paper Ib. The indication by the SAU transformation of a strong resistivity decrease within the upper mantle is due solely to the longest period estimate, and hence is not considered reliable.

6.2 Monte-Carlo models

Resistivity-depth profiles consistent with the MT responses were discovered by a modified form of the Monte-Carlo search procedure of Jones and Hutton, (1979b; see also Paper Ia). For the NAT response, it was a priori assumed that the top layer was of 10^4 Ωm, to be consistent with the information known about KIR (Westerlund, 1972). For SAU, the top layer resistivity was assumed to be 3,000 Ωm, and no models were sought in which the top layer thickness was less than 10 km, from the AMT information.

Four layer resistivity-depth profiles of models acceptable to 15 of the 16 response estimates (8 apparent resistivity and 7 phase) for NAT are illustrated in Fig. 11, and the acceptable parameter statistics are given in Table 2a. The theoretical response of the best-fitting model found by the search, listed in Table 2, is illustrated in Fig. 7. It is obvious that the upper mantle resistivity is well defined to 95 Ωm (93–99 Ωm as mean plus/minus one standard deviation of the accepted model parameter ρ_3), which is in excellent agreement with the resistivity of the upper mantle beneath KIR (Paper Ia). Also, exactly as for the KIR models, a well conducting layer, of $\rho = 2$–10 Ωm, is required below NAT at a depth of 195–225 km. This depth is somewhat greater, by about 20 km, than beneath KIR. However, models can be found for KIR and NAT for which this depth is the same beneath both locations, hence the evidence from these two locations gives only marginal support to any conjecture that the asthenosphere deepens from KIR to NAT.

For SAU, the resistivity-depth profiles of models discovered, which were acceptable to all 13 data points plus their standard errors (7 for apparent resistivity and 6 for phase), are as illustrated in Fig. 12, and the acceptable parameter statistics are given in Table 2b. The theoretical response of the best-fitting model, listed in Table 2, is illustrated in Fig. 8. The models are significantly different from those acceptable to the NAT, KIR, and KEV responses in one important detail – namely the requirement for a well conducting lower crustal layer, of $\rho = 18$–36 Ωm. At upper mantle depths, the resistivity is in the range 95–275 Ωm, which is slightly more resistive than beneath KIR and NAT, but not exceptionally so. Due to the attenuation of the

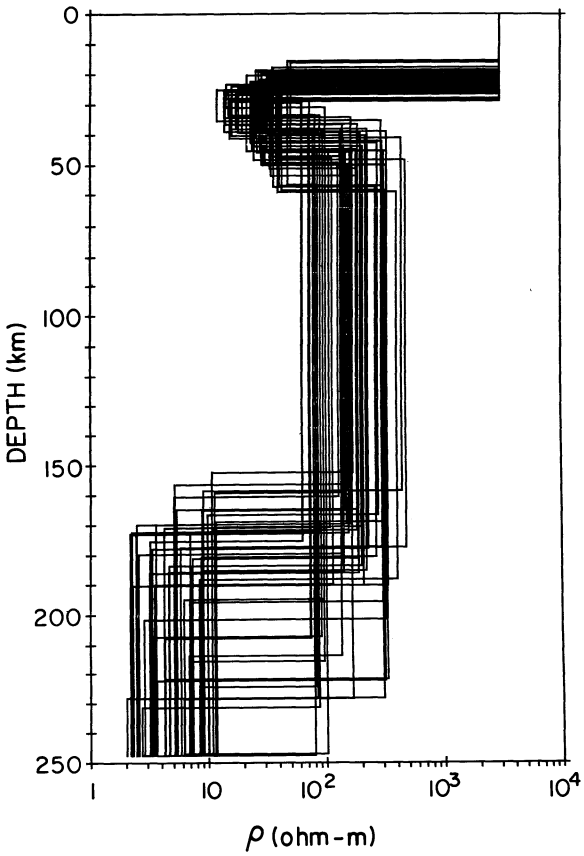

Fig. 12. The resistivity-depth profiles of models found that are acceptable to the SAU responses illustrated in Figs. 8 and 9

electromagnetic fields in the lower crustal conducting layer, of depth integrated conductivity in the range 550–900 S, penetration was not afforded to deep upper mantle depths. Hence, the structure at depths below about 150 km is not resolved, and accordingly any "electrical asthenosphere" cannot be any shallower than 150 km below SAU.

7. Discussion and conclusions

The models consistent with the MT response functions observed at NAT and SAU, as illustrated in Figs. 11 and 12, are indicative of several important factors. Basically the interpretation of the NAT magnetotelluric response is in total accord with that for the KIR HSG response (Paper Ia) – and hence the points made about the KIR models are also true for the NAT models. These are:

(1.1) The depth of the base of the top layer (14 km mean value) corresponds with the current best estimates of the upper crustal thickness, and hence this interface may be the electrical analogue of the seismic Conrad discontinuity. The implication here is that the Conrad discountinuity is associated with an electrical conductivity increase. However, as the nature of the seismic Conrad discontinuity is little understood, the accord in these depths may be purely coincidental.

(1.2) A lower crustal layer of around 300 Ωm, which is classified as Type II by Jones (1981 c).

(1.3) There is a small, or none existent, electrical resistivity contrast at the seismic Moho boundary, which concurs with the doubts of Theilen and Meissner (1979) of there being a strong acoustic interface at the Moho in this region.

(1.4) The depth of the transition to a well conducting layer, of $\rho = 2.5$–$10\,\Omega$m, in the upper mantle corresponds with seismic evidence for the existence of a low compressional wave velocity layer in the same region (see Paper Ia for details).

For the models acceptable to the SAU response, three major points are important:

(2.1) There must exist a lower crustal conducting layer, of $\rho = 18$–$36\,\Omega$m, in the region around SAU. The necessity for a conducting zone was already known from the strong attenuation of the vertical magnetic component in this region compared to northern Scandinavia (see Küppers et al., 1979, Fig. 6). For a source of wavelength 1,000 km (approximately the dominant wavelength of the electrojet illustrated in Fig. 5 of Küppers et al.) and period of 200 s (the dominant periodicity of the event displayed in Fig. 6 of Küppers et al.), the H_Z/H_X ratio in northern Scandinavia, assuming that the geoelectric structure is as given by the best-fitting models to the KIR and NAT responses, is 0.4–0.45, which is in accord with the observations at MUO (see Fig. 6 of Küppers et al.). For the SAU region however, i.e., assuming the best-fitting model to the SAU response, this ratio is 0.3, as indeed shown by station SAU in Fig. 6 of Küppers et al.. Station JOK displays a much smaller H_Z/H_X ratio, of around 0.2, which is probably caused by $2D$ effects due to the Ladoga-Bothnian Bay zone. Such a conducting lower crustal layer classifies it as Type III according to the system proposed by Jones (1981 c). The implication for seismic studies is that this lower crustal layer will exhibit a normal compressional wave velocity, of $V_P = 6.8\,\mathrm{km\,s^{-1}}$, but a low shear wave velocity, of $V_S = 3.4$–$3.7\,\mathrm{km\,s^{-1}}$, entailing a Poisson's ratio greater than 0.3. Such a zone has previously been reported for the southeastern Grenville Province of the Canadian Shield (Jordan and Frazer, 1975; Connerney and Kuckes, 1980; Connerney et al., 1980), and for the southeastern African Shield region (Block et al., 1969; van Zijl, 1977; Blohm et al., 1977). In both cases, the effects of serpentinization were postulated to explain the anomalous seismic and electromagnetic results. However, in a recent compilation of observations, Shankland and Ander (in press 1983) conjecture that these high conductivities may be due to a water-rich fluid with a strong content of conducting solutes, which suggests that the lower crust beneath the regions must have a porosity of 0.01–0.1 %.

(2.2) Beneath southern Finland there is an electrical boundary which corresponds very well with the postulated Moho depth of 46 km for the region (Bungum et al., 1980), although the Moho is believed to dip sharply, to a depth of around 55 km, beneath, and to the northeast of, the LBBZ (Luosto et al., 1982). The geoelectric interface, at a most probable depth of 42 km, is between a layer of around 25 Ωm and an underlying one of around 150 Ωm, i.e., it implies almost an order of

magnitude increase in electrical resistivity. This contrasts sharply with the models acceptable to the NAT, KIR and KEV responses which do not display any appreciable resistivity variation at Moho depths.

(2.3) Although the modified Niblett-Bostick transformation of the SAU response (Fig. 10) infers a strong resistivity decrease within the upper mantle, this is not shown to be unequivocally so by the Monte-Carlo model search procedure. Virtually any conductivity-depth distribution below 150 km is permitted by the data. However, if an electrical asthenospheric layer is present beneath southern Finland, it can be no shallower than 150 km.

A simple 2*D* model of the LBBZ is one in which the 1*D* models for SAU and for NAT are juxtaposed to represent the south-westward and north-eastward sides of the zone respectively (it cannot be stressed too highly that this is a very simplified model of the zone – but one that may indicate if a 1*D* model for SAU is valid). Assuming that the upper crust is contiguous across the zone, and is of 5,000 Ωm resistivity and 20 km thickness, the differences in the lower crustal layers are represented by two adjacent zones of 25 Ωm (for the SW side) and 250 Ωm (for the NE side) of 25 km thickness (i.e., total crustal thickness of 45 km). The mantle can also be assumed to be contiguous across the zone, with an upper mantle of 100 Ωm to a depth of 200 km, underlain by an electrical asthenosphere of 5 Ωm. For this 2*D* model, at a position corresponding to the SAU site with respect to the LBBZ, the two possible polarizations of the incident field yield apparent resistivities and phases of 75 Ωm and 43° (*E*-polarization) and 53 Ωm and 51° (*B*-polarization) at a period of 1,000 s. The 1*D* model for the SAU side of the fault yields MT response values of 69 Ωm and 45°. At 100 s, these responses are 80 Ωm and 63° (*E*), 84 Ωm and 65° (*B*), and 89 Ωm and 67° (1*D*) respectively. Hence, given the errors in the data, it is not possible at SAU to detect the effects of the above described simplified LBBZ model.

As mentioned in the Introduction, there have been other geomagnetic induction studies conducted in Finland by collaborative efforts on the part of groups from Finland (Oulu), Hungary (Sopron) and the USSR (Moscow). Ádám et al., (1982) made measurements at five locations on a profile crossing the LBBZ, from SW to NE, with an average interstation separation of some 60 km. The response functions from all stations exhibited a large anisotropy between the rotated maximum apparent resistivity, ρ_{max}, and the rotated minimum apparent resistivity, ρ_{min}, at all frequencies. The closest station to SAU, MT1 (which was their south-westernmost station, and was approximately 100 km north of SAU), displayed a very high anisotropy, of greater than 2 orders of magnitude, throughout the whole period range of observation. This was interpreted by the authors as due to the effects of a narrow tectonic zone (dyke), filled with well-conducting formations, embedded in the resistive host (of resistivity 10^4 Ωm). In stark contrast, the apparent resistivities for SAU show *no* anisotropy, and, as mentioned previously, the authors believe that they are fully justified in undertaking a 1*D* interpretation of the response function.

Ádám et al. (1983), supplimenting the above study with 2 long period MT observations (10^4–10^5 s), show ρ_{max} and ρ_{min} curves for one of them that are almost parallel, on a log-scale, but displaced by an order of magnitude. This feature is taken to suggest that surface telluric distortion effects are responsible, of the type discussed by Richards et al. (1982). As discussed previously, such a distortion is not possible at SAU due to the excellent accord between the HSG and MT response functions (telluric distortion effects, due to near-surface inhomogeneities, would adversely affect the MT response but not the HSG one, as no telluric field is measured).

Finally, in the prelimenary interpretation of their magnetometer array data, Pajunpää et al. (in press 1983) concluded that there is probably a difference in electrical conductivity beneath the western part, compared to the north-eastern part, of their array. Their array straddled the LBBZ, and hence this difference may be attributable to the better conducting lower crust to the SW of the fault compared to the NE of it.

Acknowledgements. One of the authors (AGJ) was supported by grants from the Deutsche Forschungsgemeinschaft whilst in Münster, was a guest of the Swedish Geological Survey for five months, and has been supported by Natural Sciences and Engineering Research Council of Canada grants to Professors G.D. Garland (NSERCC A2115), R.N. Edwards and G.F. West (NSERCC G0501) whilst at Toronto – he wishes to express his appreciation to all three bodies. Another author (BO) is employed at the Swedish Geological Survey, and is grateful to that organisation for support during all phases of this project. JT is in the employ of the Geophysics Department of Oulu University, and is thankful to all members of the department for guidance.

The authors are indebted to Professor J. Untiedt (Münster) for many positive comments on a earlier version of this manuscript. The generous advice from Professors S.E. Hjelt (Oulu) and G.D. Garland (Toronto) was also very useful and much appreciated.

References

Ádám, A., Kaikkonen, P., Hjelt, S.E., Pajunpää, K. Szarka, L., Verö, J., Wallner, Â.: Magnetotelluric and audiomagnetotelluric measurements in Finland. Tectonophys. **90**, 77–90, 1982

Ádám, A., Vanyan, L.L., Hjelt, S.E., Kaikkonen, P., Shilovsky, P.P., Palshin, N.A.: A comparison of deep geoelectric structure in the Pannonian basin and the Baltic shield. J. Geophys., this issue, 1983

Beamish, D.: Diurnal characteristics of transfer functions at pulsation periods. Geophys. J.R. Astron. Soc. **61**, 623–643, 1980

Bendat, J.S., Piersol, A.G.: Random data: analysis and measurement procedures. New York: Wiley-Interscience 1971

Benderitter, Y., Ngoc Thach, H., Jolivet, A.: Magnetotelluric method for mining exploration. Contributed paper at "35th EAEG", held in Brighton, on June 1973, 27pp., mimeographed, 1973

Bentley, C.R.: Error estimation in two dimensional magnetotelluric analyses. Phys. Earth Planet. Inter. **7**, 423–430, 1973

Bingham, C., Godfrey, M.D., Tukey, J.W.: Modern techniques for power spectrum estimation. IEEE Trans. Audio Electroacoust. **AU-15**, 56–66, 1967

Block, S., Hales, A.L., Landisman, M.: Velocities in the crust

and upper mantle of southern Africa from multi-mode surface wave dispersion. Bull. Seismol. Soc. Am. **59**, 1599–1629, 1969

Blohm, E.K., Worzyk, P., Scriba, H.: Geoelectrical deep soundings in southern Africa using the Cabora Bassa power line. J. Geophys. **43**, 665–679, 1977

Bostick, F.X.: A simple almost exact method of MT analysis. In: Workshop on Electrical Methods in Geothermal Exploration, U.S. Geol. Surv., Contract No. 14080001-8-359, 1977

Bungum, H., Pirhonen, S.E., Husebye, E.S.: Crustal thickness in Fennoscandia. Geophys. J.R. Astron. Soc. **63**, 759–774, 1980

Carter, G.C.: Bias in magnitude-squared coherence estimation due to misalignment. IEEE Trans. Acoust., Speech, Signal Processing **ASSP-28**, 97–99, 1980

Chave, A.D., von Herzen, R.P., Poehls, K.A., Cox, C.S.: Electromagnetic induction fields in the deep ocean north-east of Hawaii: implications for mantle conductivity and source fields. Geophys. J.R. Astron. Soc. **66**, 379–406, 1981

Connerney, J.E.P., Kuckes, A.F.: Gradient analysis of geomagnetic fluctuations in the Adirondacks. J. Geophys. Res. **85**, 2615–2624, 1980

Connerney, J.E.P., Nekut, A., Kuckes, A.F.: Deep crustal electrical conductivity in the Adirondacks. J. Geophys. Res. **85**, 2603–2614, 1980

Cox, C.S., Filloux, J.H., Gough, D.I., Larsen, J.C., Poehls, K.A., von Herzen, R.P., Winter, R.: Atlantic lithospheric sounding. In: Electromagnetic Induction in the Earth and Moon, U. Schmucker, ed.: pp. 13–22. Centr. Acad. Publ. Japan, Tokio and D. Reidel Publ. Co., Dordrecht, 1980

Dmitriev, V.I., Berdichevsky, M.N.: The fundamental model of magnetotelluric sounding. Proc. IEEE **67**, 1034–1044, 1979

Filloux, J.H.: North Pacific magnetotelluric experiments. In: Electromagnetic Induction in the Earth and Moon, U. Schmucker, ed.: pp. 33–43. Centr. Acad. Publ. Japan, Tokio and D. Reidel Publ. Co., Dordrecht, 1980

Fischer, G., Schnegg, P.-A.: The dispersion relations of the magnetotelluric response and their incidence on the inversion problem. Geophys. J.R. Astron. Soc. **62**, 661–673, 1980

Fournier, H.G., Febrer, J.: Gaussian character of the distribution of magnetotelluric results working in log-space. Phys. Earth Planet. Inter. **12**, 359–364, 1976

Fowler, R.A., Kotick, B.J., Elliot, R.D.: Polarisation analysis of natural and artificially induced geomagnetic micropulsations. J. Geophys. Res. **72**, 2871–2883, 1967

Glaßmeier, K.-H.: Magnetometer array observations of a giant pulsation event. J. Geophys. **48**, 127–138, 1980

Goodman, N.R.: Measurement of matrix frequency response functions and multiple coherence functions. AFFDL TR 65-56, Air Force Flight Dynamics Lab., Wright-Patterson AFB, Ohio, 1965

Gough, D.I., Reitzel, J.S.: A portable three component magnetic variometer. J. Geomagn. Geoelectr. **19**, 203–215, 1967

Greenwald, R.A., Weiss, W., Nielsen, E., Thomson, N.R.: STARE: a new radar auroral backscatter experiment in northern Scandinavia. Radio Sci. **13**, 1021–1039, 1978

Hald, A.: Statistical Theory with Engineering Applications. New York: John Wiley 1952

Jeffrey, A.: Mathematics for Engineers and Scientists. London: Nelson 1971

Jones, A.G.: Geomagnetic Induction Studies in Southern Scotland. Ph. D. thesis, Dept. of Geophysics, Edinburgh Univ., Edinburgh, Scotland, 1977

Jones, A.G.: Geomagnetic induction studies in Scandinavia – I. Determination of the inductive response function from the magnetometer data. J. Geophys. **48**, 181–194, 1980

Jones, A.G.: Geomagnetic induction studies in Scandinavia – II. Geomagnetic depth sounding, induction vectors and coast effect. J. Geophys. **50**, 23–36, 1981a

Jones, A.G.: Transformed coherence functions for multivariate studies. IEEE Trans. Acoust., Speech, Signal Processing **ASSP-29**, 317–319, 1981b

Jones, A.G.: On a type classification of lower crustal layers under Precambrian regions. J. Geophys. **49**, 226–233, 1981c

Jones, A.G.: On the electrical crust-mantle structure in Fennoscandia: no Moho and the asthenosphere revealed? Geophys. J.R. Astron. Soc. **68**, 371–388, 1982a

Jones, A.G.: Observations of the electrical asthenosphere beneath Scandinavia. Tectonophys. **90**, 37–55, 1982b

Jones, A.G.: On the equivalence of the "Niblett" and "Bostick" transformations in the magnetotelluric method. J. Geophys. **53**, 72–73, 1983a

Jones, A.G.: The electrical structure of the lithosphere and asthenosphere beneath the Fennoscandian shield. J. Geomagn. Geoelectr., in press 1983b

Jones, A.G.: The problem of "current channelling": a critical review. Geophys. Surv., in press 1983c

Jones, A.G., Hutton, R.: A multi-station magnetotelluric study in southern Scotland – I. Fieldwork, data analysis and results. Geophys. J.R. Astron. Soc. **56**, 329–349, 1979a

Jones, A.G., Hutton, R.: A multi-station magnetotelluric study in southern Scotland – II. Monte-Carlo inversion of the data and its geophysical and tectonic implications. Geophys. J.R. Astron. Soc. **56**, 351–368, 1979b

Jordan, T.H., Frazer, L.N.: Crustal and upper mantle structure from S_p phases. J. Geophys. Res. **80**, 1504–1518, 1975

Küppers, F., Post, H.: A second generation Gough-Reitzel magnetometer. J. Geomagn. Geoelectr. **33**, 225–237, 1981

Küppers, F., Untiedt, J., Baumjohann, W., Lange, K., Jones, A.G.: A two-dimensional magnetometer array for ground-based observations of auroral zone electric currents during the International Magnetospheric Study (IMS). J. Geophys. **46**, 429–450, 1979

Kulhánek, O.: Introduction to Digital Filtering. Amsterdam: Elsevier 1976

Kurtz, R.D., Garland, G.D.: Magnetotelluric measurements in eastern Canada. Geophys. J.R. Astron. Soc. **45**, 321–347, 1976

Lilley, F.E.M.: Magnetometer array studies: a review of the interpretation of observed fields. Phys. Earth Planet. Inter. **10**, 231–240, 1975

Luosto, U., Lanne, E., Korhonen, H., Guterch, A., Grad, M., Materzok, R., Pajchel, J., Perchuc, E., Yliniemi, J.: Results of the deep seismic sounding of the Earth's crust on the profile SVEKA. Contributed paper at 18th. General Assembly of the E.S.C., held in Leeds, U.K., 1982

Mareschal, M.: Source effects and the interpretation of geomagnetic sounding data at sub-auroral latitudes. Geophys. J.R. Astron. Soc. **67**, 125–136, 1981

Niblett, E.R., Sayn-Wittgenstein, C.: Variation of the electrical conductivity with depth by the magnetotelluric method. Geophysics **25**, 998–1008, 1960

Nuttall, A.H., Carter, G.C.: Bias the estimate of magnitude-squared coherence. IEEE Trans. Acoust., Speech, Signal Processing, **ASSP-24**, 582–583, 1976

Pajunpää, K., Heikka, J., Korja, T.: Magnetometer array studies in Finland. J. Geomagn. Geoelectr., in press 1983

Parker, R.L.: The inverse problem of electrical conductivity in the mantle. Geophys. J.R. Astron. Soc. **22**, 121–138, 1970

Parker, R.L.: The inverse problem of electromagnetic induction: existence and construction of solutions based on incomplete data. J. Geophys. Res. **85**, 4421–4425, 1980

Rader, C.M.: An improved algorithm for high speed autocorrelation with applications to spectral estimation. IEEE Trans. Audio Electroacoust. **AU-18**, 439–441, 1970

Reddy, I.K., Rankin, D.: On the interpretation of magnetotel-

luric data in the plains of Alberta. Can. J. Earth Sci. **9**, 514–527, 1972

Reddy, I.K., Rankin, D.: Coherence functions for magnetotelluric analysis. Geophysics **39**, 312–320, 1974

Reddy, I.K., Phillips, R.J., Whitcomb, J.H., Cole, C.M., Taylor, R.A.: Monitoring of time-dependent electrical resistivity by magnetotellurics. J. Geomagn. Geoelectr. **28**, 165–178, 1976

Richards, M.L., Schmucker, U., Steveling, E.: Electrical conductivity studies in the Urach geothermal area with special regard to distortion effects of telluric currents. Contributed paper at 6th Workshop on Electromagnetic Induction in the Earth and Moon, held in Victoria, B.C., on August 15–22, 1982

Richmond, A., Baumjohann, W.: Three-dimensional analysis of magnetometer array data. J. Geophys., in press 1983

Rooney, D., Hutton, V.R.S.: A magnetotelluric and magnetovariational study of the Gregory Rift Valley, Kenya. Geophys. J.R. Astron. Soc. **51**, 91–119, 1977

Schmucker, U.: Induktion in geschichteten Halbräumen durch inhomogene Felder. In: Protokoll über das Kolloquium „Elektromagnetische Tiefenforschung" in Berlin-Lichtenrade vom 1.–3. April 1980, V. Haak and J. Homilius, eds.: pp 197–210. Niedersächsisches Landesamt für Bodenforschung, Hannover 1980

Shankland, T.J., Ander, M.E.: Electrical conductivity, temperatures, and fluids in the lower crust. J. Geophys. Res., in press 1983

Shanks, J.L.: Recursion filters for digital processing. Geophysics **32**, 33–51, 1967

Sims, W.E., Bostick, F.X.: Methods of magnetotelluric analysis. Elec. Geophys. Res. Lab. Tech. Rep. **58**, Univ. Texas at Austin, 1969

Sims, W.E., Bostick, F.X., Smith, H.W.: The estimation of magnetotelluric tensor elements from measured data. Geophysics **36**, 938–942, 1971

Swift, C.M.: A Magnetotelluric Investigation of an Electrical Conductivity Anomaly in the South-Western United States. Ph.D. thesis, Dept. Geology and Geophys., M.I.T., Cambridge, Mass., 1967

Theilen, Fr., Meissner, R.: A comparison of crustal and upper mantle features in Fennoscandia and the Rhenish shield, two areas of recent uplift. Tectonophys. **61**, 227–242, 1979

van Zijl, J.S.V.: Electrical studies of the deep crust in various tectonic provinces of southern Africa. In: The Earth's Crust: Its Nature and Physical Properties, J.G. Heacock, ed.: pp 470–450. Geophys. Monogr. Ser., vol. 20, 1977

Vanyan, L.L., Berdichevsky, M.N., Fainberg, E.B., Fiskina, M.V.: The study of the asthenosphere of the East European platform by electromagnetic sounding. Phys. Earth Planet. Inter. **14**, P1-P2 (Letter section), 1977

Vanyan, L.L., Berdichevsky, M.N., Vasin, N.D., Okulyessky, B.A., Shilovsky, P.P.: On the normal geoelectric profile. Izvestiya, Earth Physics, **16**, 131–133, 1980

Vozoff, K.: The magnetotelluric method in the exploration of sedimentary basins. Geophysics **37**, 98–141, 1972

Weidelt, P.: The inverse problem of geomagnetic induction. Z. Geophys. **38**, 257–289, 1972

Weidelt, P., Müller, W., Losecke, W., Knödel, K.: Die Bostick transformation. In: Protokoll über das Kolloquium „Elektromagnetische Tiefenforschung" in Berlin-Lichtenrade vom 1.–3. April 1980, V. Haak and J. Homilius, eds.: pp 227–230. Niedersächsisches Landesamt für Bodenforschung, Hannover, 1980

Welch, P.D.: The use of fast Fourier transform for the determination of power spectra: a method based on time averaging over short, modified periodograms. IEEE Trans. Audio Electroacoust., **AU-15**, 70–73, 1967

Westerlund, S.: Magnetotelluric experiments in the frequency range 0.01 Hz to 10 kHz. KGO Report, **72:10**, Kiruna Geophysical Observatory, 1972

Whalen, J.A.: Auroral oval plotter and nomogram for determining corrected geomagnetic local time, latitude, and longitude for high latitudes in the northern hemisphere. Environ. Res. Paper No. 327, Air Force Cambridge Res. Lab., Bedford, Mass., 1970

Received May 5, 1983; Revised July 7, 1983;
Accepted July 28, 1983